www.nature.com/cdd

CDDpress

ARTICLE

CD63 acts as a functional marker in maintaining hematopoietic stem cell quiescence through supporting TGFβ signaling in mice

Mengjia Hu[1], Yukai Lu[1], Song Wang[1], Zihao Zhang[1], Yan Qi[1], Naicheng Chen[1], Mingqiang Shen[1], Fang Chen[1], Mo Chen[1], Lijing Yang[1], Shilei Chen[1], Dongfeng Zeng[2], Fengchao Wang[1], Yongping Su[1], Yang Xu[1✉] and Junping Wang[1✉]

Hematopoietic stem cell (HSC) fate is tightly controlled by various regulators, whereas the underlying mechanism has not been fully uncovered due to the high heterogeneity of these populations. In this study, we identify tetraspanin CD63 as a novel functional marker of HSCs in mice. We show that CD63 is unevenly expressed on the cell surface in HSC populations. Importantly, HSCs with high CD63 expression ($CD63^{hi}$) are more quiescent and have more robust self-renewal and myeloid differentiation abilities than those with negative/low CD63 expression ($CD63^{-/lo}$). On the other hand, using CD63 knockout mice, we find that loss of CD63 leads to reduced HSC numbers in the bone marrow. In addition, CD63-deficient HSCs exhibit impaired quiescence and long-term repopulating capacity, accompanied by increased sensitivity to irradiation and 5-fluorouracil treatment. Further investigations demonstrate that CD63 is required to sustain TGFβ signaling activity through its interaction with TGFβ receptors I and II, thereby playing an important role in regulating the quiescence of HSCs. Collectively, our data not only reveal a previously unrecognized role of CD63 but also provide us with new insights into HSC heterogeneity.

Cell Death & Differentiation (2022) 29:178–191; https://doi.org/10.1038/s41418-021-00848-2

INTRODUCTION

Hematopoietic stem cells (HSCs) play a central role in maintaining the homeostasis of the hematopoietic system by balancing their ability to self-renew and differentiate throughout an organism's lifetime [1, 2]. Adult HSCs mainly reside in a specialized microenvironment (niche) located in the bone marrow (BM) [3, 4]. Under normal conditions, only a small percentage of HSCs are progressing through the cell cycle [5, 6]. Maintenance of quiescence is recognized as a fundamental characteristic of HSCs, which is essential for preserving the stem cell pool [3, 7]. Studies have shown that HSC biology is coordinately regulated by cytokines/cytokine receptors, signal transduction molecules, transcription factors, cell cycle regulators, etc [1, 8]. However, the underlying molecular mechanism is still not fully understood due to the high heterogeneity of HSC populations [9, 10].

The evidence suggests that phenotypically homogeneous HSCs exhibit diverse characteristics, including cell cycle status, metabolic profile, location, lineage reconstitution potential, and response to external stimuli [11, 12]. Currently, why HSC subtypes exist, how they develop and how new subpopulations can be identified remain hot topics in the stem cell field. Transforming growth factor β (TGFβ) signaling controls a wide spectrum of cell biological processes [13]. Previous studies using various mouse models have indicated that TGFβ signaling plays a vital role in the regulation of HSC behaviors, including quiescence, self-renewal and differentiation [14–17]. Intriguingly, distinct HSC subpopulations respond differently to TGFβ in the BM [18]. However, relatively little is known about how to coordinate TGFβ signaling in HSC compartments.

A number of studies using surface markers or reporter genes have defined several HSC subpopulations with different functions [19–21]. However, recent single-cell transcriptional profiling data indicate that our understanding of the biological features of HSCs is still inadequate [9, 22]. Therefore, identifying new HSC markers may provide new insights into the heterogeneity of HSCs. CD63 is a member of the tetraspanin family that is distinguished by its four transmembrane domains [23]. In addition to being an indicator of the activation of several blood cells [24, 25], CD63 has many pathological and physiological functions [21, 25, 26]. CD63 can associate with its interaction partners, such as integrins, receptors, kinases, and other tetraspanin proteins, on the cell surface, thereby contributing to the regulation of multiple signaling pathways [23, 24, 26, 27]. Of note, CD63 has also been shown to be present in human and mouse HSCs [28, 29], whereas its exact role in HSCs remains to be established.

In the present study, we first found that CD63 exhibits a heterogeneous expression pattern in mouse HSCs and that

[1]State Key Laboratory of Trauma, Burns and Combined Injury, Institute of Combined Injury, Chongqing Engineering Research Center for Nanomedicine, College of Preventive Medicine, Third Military Medical University, Chongqing, China. [2]Department of Hematology, Daping Hospital, Third Military Medical University, Chongqing, China. ✉email: xyzq2023@163.com; wangjunping@tmmu.edu.cn

Edited by D. Aberdam

Received: 31 March 2021 Revised: 28 July 2021 Accepted: 29 July 2021
Published online: 6 August 2021

$CD63^{high}$ ($CD63^{hi}$) HSCs are more quiescent and exhibit more robust self-renewal ability than $CD63^{-/low}$ ($CD63^{-/lo}$) HSCs. Furthermore, deletion of CD63 was found to decrease HSC numbers and impair their quiescence and function. Mechanistically, CD63 supports TGFβ signaling activity by interacting with TGFβ receptors I and II, which are involved in regulating the quiescence of HSCs. Collectively, our findings identify CD63 as a functional marker of HSCs and reveal a new mechanism for modulating TGFβ signaling.

RESULTS

CD63 is unevenly distributed on the cell surface in HSC populations and its high expression identifies more quiescent HSCs

Previous studies have identified multiple markers of HSCs, but there are still many molecules that have not been studied. We thus reanalyzed single-cell RNA-sequencing (scRNA-seq) data from murine hematopoietic stem progenitor cells (HSPCs) that were sorted by flow cytometry. After quality control and principal component analysis (PCA), the first 13 PCs were determined by ElbowPlot and used for subsequent analysis (Supplementary Fig. S1A–C). We identified 11 distinct cell clusters (Fig. 1A), similar to the findings of a previous study [30]. Among the differentially expressed genes, we noticed that both CD63 and CD81 were more abundant in the most primitive HSC population (C1 clusters) compared with other unprimed HSPCs (C2 and C3 clusters) (Fig. 1B). Since the potential role of CD81 in HSCs has been disclosed [31], we then focused mainly on CD63. Consistent with the above result, the expression of CD63 was higher in purified long-term HSCs (LT-HSCs) than in all multipotent progenitor (MPP) populations (Fig. 1C). A similar result was obtained from another public single-cell RNA-seq database (Supplementary Fig. S2A) [32]. Considering that CD63 is localized at the plasma membrane and lysosomal membrane, we analyzed its subcellular distribution by flow cytometry with surface and intracellular staining. Interestingly, CD63 predominantly displayed intracellular localization in mature BM cells, while approximately half of the CD63 content was present on the cell surface in HSPCs (Fig. 1D, E and Supplementary Fig. S2E). These data also confirmed the higher cell surface expression of CD63 in LT-HSCs than in other LSK ($Lineage^-$ $c\text{-}Kit^+$ $Sca1^+$) subsets (Fig. 1D, E and Supplementary Fig. S2E). Alternatively, LT-HSCs were more enriched in $CD63^+$ than in $CD63^-$ LSKs (Fig. 1F). Similar results were obtained by using the signaling lymphocytic activation molecule (SLAM) markers CD48 and CD150 (Supplementary Fig. S2F). Moreover, the scRNA-seq data showed that CD63 was expressed to a greater degree in myeloid-primed clusters (Fig. 1B), which was in line with the finding from flow cytometric analysis (Fig. 1D, E).

Next, we asked whether HSCs with different levels of CD63 have distinct properties. Given that HSCs exist on a continuous CD63 expression, we therefore gated the top 30% and bottom 30% of CD63 expression in order to obtain pure and distinct populations of HSCs (hereafter referred to as $CD63^{-/lo}$ and $CD63^{hi}$ HSCs) (Fig. 1G). Interestingly, cell cycle analysis revealed that $CD63^{hi}$ LT-HSCs were more frequently in the G0 phase than $CD63^{-/lo}$ LT-HSCs, suggesting that $CD63^{hi}$ subpopulations are more quiescent (Fig. 1H). The same trend was observed for short-term HSCs (ST-HSCs) and MPPs, albeit to a lesser extent (Supplementary Fig. S2G). Consistently, 5-bromodeoxyuridine (BrdU) incorporation was significantly higher in $CD63^{-/lo}$ HSCs than in $CD63^{hi}$ HSCs in vivo (Fig. 1I and Supplementary Fig. S2H). However, the apoptosis rates of $CD63^{-/lo}$ and $CD63^{hi}$ HSCs were comparable (Fig. 1J and Supplementary Fig. S2I). These results suggest that although mouse HSCs are typically enriched in the $CD34^-$ $Flk2^-$ LSK compartment, coexpression of a high level of CD63 may further discriminate more quiescent HSCs.

$CD63^{hi}$ LT-HSCs display more robust self-renewal and myeloid differentiation ability

The differences in the cell cycle status of $CD63^{-/lo}$ and $CD63^{hi}$ HSCs prompted us to assess whether CD63 expression may be related to the functional properties of HSCs. We then purified $CD63^{-/lo}$ and $CD63^{hi}$ LT-HSCs by flow cytometry and evaluated their function in vitro. Unlike $CD63^{hi}$ HSCs, $CD63^{-/lo}$ HSCs could not be maintained in a liquid medium after 10 days of culture (Fig. 2A, B), accompanied by increased apoptosis rate (Supplementary Fig. S3A). Additionally, $CD63^{hi}$ LT-HSCs displayed stronger colony-forming ability in methylcellulose medium (Fig. 2C). Next, we performed a transplantation assay using purified $CD63^{-/lo}$ and $CD63^{hi}$ LT-HSCs to determine their functional differences in vivo (Fig. 2D). Specifically, $CD63^{hi}$ LT-HSCs exhibited greater long-term repopulation potential and higher myeloid output than $CD63^{-/lo}$ LT-HSCs (Fig. 2E–H). Increased CD63 expression was actually observed in aged HSCs (Supplementary Fig. S3B, C), which are definitely biased toward myeloid differentiation [33, 34]. Furthermore, using RNA-sequencing (RNA-seq) analysis, we found a distinct difference in the $CD63^{-/lo}$ and $CD63^{hi}$ LT-HSC transcript profiles, in which 650 genes were downregulated and 361 genes were upregulated in $CD63^{hi}$ *vs* $CD63^{-/lo}$ LT-HSCs (Fig. 2I). It is not surprising that the transcription levels of myeloid-associated genes (such as Vwf, Hdc, Csf1r, Elane and Hp [19, 35–37]) were significantly increased in $CD63^{hi}$ LT-HSCs (Fig. 2I). More importantly, gene set enrichment analysis (GSEA) showed that HSC signature, quiescence and long-term gene sets were enriched in $CD63^{hi}$ LT-HSCs, whereas HSC proliferation, cell cycle and DNA duplication gene sets were enriched in $CD63^{-/lo}$ LT-HSCs (Fig. 2J). Consistent with the above data, compared with $CD63^{hi}$ LT-HSCs, $CD63^{-/lo}$ LT-HSCs revealed significant enrichment of genes associated with metabolic and biosynthetic processes (Supplementary Fig. S3D), which were further confirmed by detection of mitochondrial activity and protein synthesis rate, respectively (Fig. 2K–M). On the other hand, neither the in vitro nor in vivo functions of HSCs were significantly affected after anti-CD63 antibody (clone NVG-2) treatment (Supplementary Fig. S3E–L). Taken together, these findings show that CD63, in combination with surrogate HSC markers, may distinguish HSCs with more robust self-renewal ability.

Knockout of CD63 results in a reduced number of HSCs in mice

To clarify whether CD63 is functional or only a passive marker for HSCs, we used a CD63 knockout ($CD63^{-/-}$) mouse model. Deletion of CD63 in HSCs from $CD63^{-/-}$ mice was verified by flow cytometry (Fig. 3A). In line with previous studies [24, 38], CD63 ablation did not significantly affect the total cell number in the BM and peripheral blood (PB) of mice (Supplementary Fig. S4A, B). Further flow cytometric analysis showed that CD63 deficiency did not significantly affect the percentage and absolute number of BM LSKs and myeloid progenitors (MPs) (Fig. 3B–D). Interestingly, the percentages and absolute numbers of LT-HSCs and ST-HSCs, rather than MPPs, were modest but statistically significantly reduced when CD63 was deleted (Fig. 3E, F). Loss of HSCs in $CD63^{-/-}$ mice was further verified using CD150 and CD48 staining (Fig. 3G and Supplementary Fig. S4C). However, the percentages and numbers of hematopoietic progenitors, including GMPs, CMPs, MEPs, and CLPs, were similar between wild-type (WT) and $CD63^{-/-}$ mice (Fig. 3H and Supplementary Fig. S4D). These findings illustrate that CD63 deficiency leads to a loss of HSC number in mice.

Deletion of CD63 leads to impairment of HSC quiescence

In view of the above findings that CD63 expression is associated with HSC quiescence, we next sought to evaluate whether CD63 deletion affects cell cycle progression in HSCs. Indeed, after CD63 knockout, the percentage of HSCs in the G0 phase was reduced, whereas the percentages of HSCs in the G1 and S/G2/M phases were increased (Fig. 4A). Significantly increased proliferation of

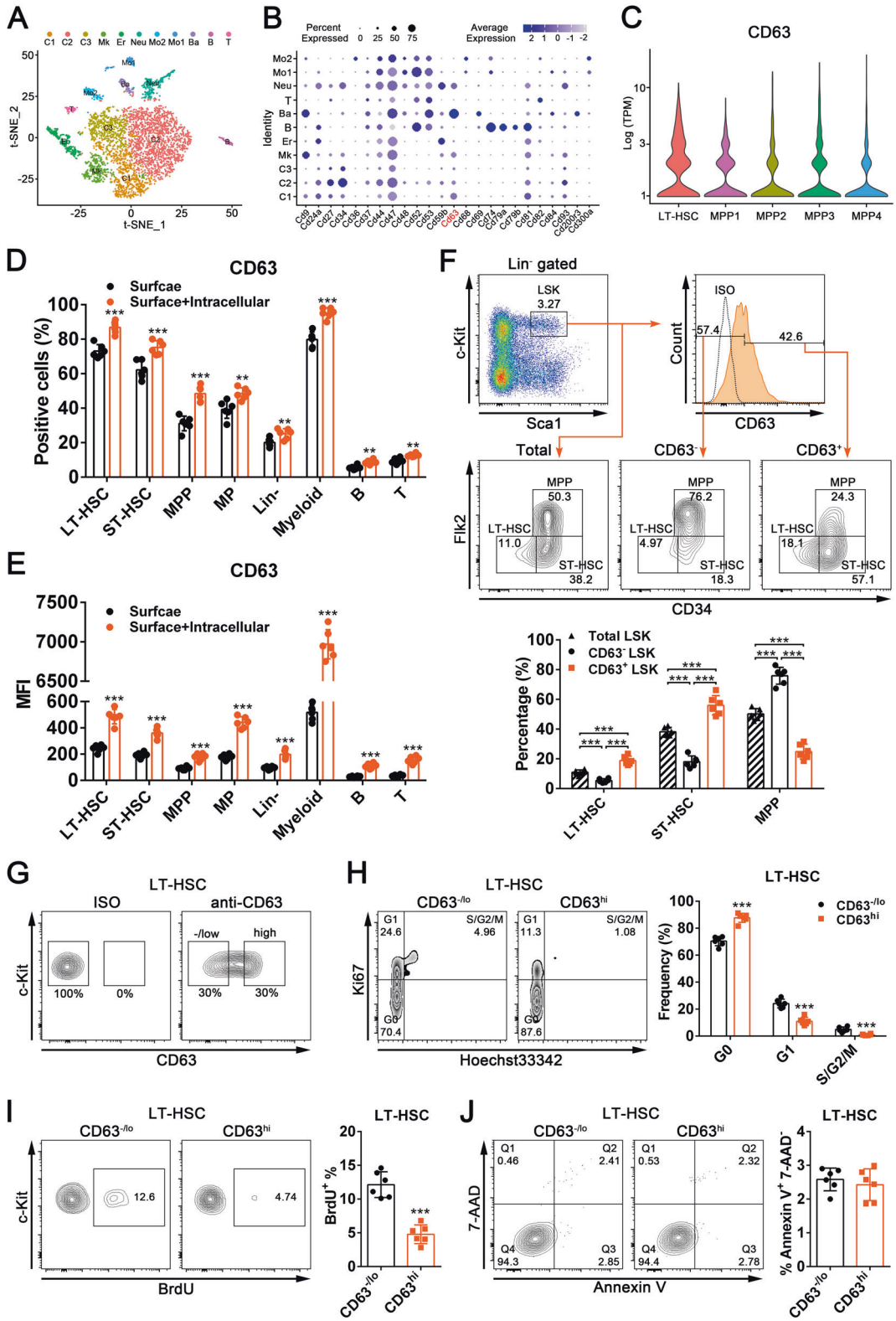

$CD63^{-/-}$ HSCs was also observed by an in vivo BrdU incorporation assay (Fig. 4B). It has been well established that proliferative cells are extremely sensitive to ionizing radiation injury [39, 40]. As expected, $CD63^{-/-}$ mice were more susceptible to death than WT mice after 6.5 Gy total body irradiation (TBI) (Fig. 4C). Meanwhile, irradiated $CD63^{-/-}$ mice displayed a more significant increase in apoptosis and DNA damage in HSCs, as well as reduced HSPC numbers (Fig. 4D–G). Consistent with these results, $CD63^{-/-}$ mice were also more sensitive to treatment with 5-fluorouracil (5-FU) (Supplementary Fig. S5A-C), a chemotherapeutic drug that preferentially eliminates cycling cells [41]. These data indicate that CD63 deficiency impairs the quiescence of HSCs.

Fig. 1 CD63 is unevenly distributed on the cell surface in HSC populations and its high expression identifies more quiescent HSCs. **A** Identification of 11 different cell clusters in HSPCs based on t-distributed stochastic neighbor embedding (t-SNE) analysis from published scRNA-seq data (GEO accession number: GSE90742). C1-C3, unprimed HSPC populations; Mk, megakaryocyte-primed progenitors; Er, erythrocyte-primed progenitors; Neu, neutrophile-primed progenitors; Mo1, type I macrophage-primed progenitors; Mo2, type II macrophage-primed progenitors; Ba, basophilia-primed progenitors; B, B cell-primed progenitors; T, T cell-primed progenitors. **B** Dot maps showing the differentially expressed genes in 11 identified clusters from Fig. 1A. **C** Violin plots showing the expression level of CD63 mRNA in purified LT-HSC, MPP1, MPP2, MPP3, and MPP4 (all these populations were combined within (**A**). **D**, **E** Flow cytometric analysis of surface and total (surface + intracellular) expression of CD63 in long-term HSCs (LT-HSCs; Lin^- c-Kit^+ $Sca1^+$ $CD34^-$ $Flk2^-$), short-term HSCs (ST-HSCs; Lin^- c-Kit^+ $Sca1^+$ $CD34^+$ $Flk2^-$) and multipotent progenitors (MPPs; Lin^- c-Kit^+ $Sca1^+$ $CD34^+$ $Flk2^+$), myeloid progenitors (MPs; Lin^- c-Kit^+ $Sca1^-$), Lin^- cells ($Lineage^-$), myeloid cells ($CD11b^+$ $Gr\text{-}1^+$), B cells ($B220^+$) and T cells ($CD3e^+$) from the BM of normal mice ($n = 6$). The positive percentage and MFI of CD63 are shown in (**D**) and (**E**), respectively. Data are shown as the mean ± SD. $^{**}P < 0.01$, $^{***}P < 0.001$. MFI, mean fluorescence intensity. **F** Flow cytometric analysis of the percentages of LT-HSCs, ST-HSCs, and MPPs in total, $CD63^-$ and $CD63^+$ LSKs from the BM of normal mice by surface staining ($n = 6$). Representative flow cytometric plots are shown in the top panel. Data are shown as the mean ± SD. $^{***}P < 0.001$. ISO, isotype control. **G** Gating strategies used for subsequent flow cytometric analysis and sorting of $CD63^{-/low}$ ($CD63^{-/lo}$) and $CD63^{high}$ ($CD63^{hi}$) LT-HSCs. **H** Flow cytometric analysis of the cell cycle status of $CD63^{-/lo}$ and $CD63^{hi}$ LT-HSCs from the BM of normal mice ($n = 6$). Representative flow cytometric plots are shown in the left. Data are shown as the mean ± SD. $^{***}P < 0.001$. **I** Flow cytometric analysis of the in vivo BrdU incorporation of $CD63^{-/lo}$ and $CD63^{hi}$ LT-HSCs from the BM of normal mice ($n = 6$). Representative flow cytometric plots are shown in the left. Data are shown as the mean ± SD. $^{***}P < 0.001$. **J** Flow cytometric analysis of the apoptosis of $CD63^{-/lo}$ and $CD63^{hi}$ LT-HSCs from the BM of normal mice ($n = 6$). Representative flow cytometric plots are shown in the left. Data are shown as the mean ± SD.

Loss of CD63 compromises the long-term repopulating ability of HSCs

Cell cycle quiescence is hypothesized to underlie HSC self-renewal and engraftment potential [42, 43]. In consideration of this, we carried out a competitive BM transplantation (BMT) assay (Fig. 5A). BM cells obtained from WT or $CD63^{-/-}$ mice were mixed with CD45.1 mice BM cells at a ratio of 1:1 and were then transplanted into lethally irradiated CD45.1 mice. As anticipated, CD63 deficiency resulted in a significant decrease in the long-term repopulation ability of HSCs (Fig. 5B, C and Supplementary Fig. S6B). More obvious changes were observed with secondary BMT, accompanied by lymphoid-biased differentiation (Fig. 5D, E and Supplementary Fig. S6B). Furthermore, we performed another transplantation assay using purified LT-HSCs, as shown in Fig. 5F. The greatly impaired long-term repopulation ability of HSCs and biased lineage distribution was also observed in recipients reconstituted with $CD63^{-/-}$ LT-HSCs (Fig. 5G–J and Supplementary Fig. S6C). Specifically, the compromised function of HSCs induced by CD63 deletion was not due to homing defects (Supplementary Fig. S6D, E). In addition, reciprocal BMT assays showed that the role of CD63 in HSCs was cell intrinsic rather than microenvironment dependent (Fig. 5K–M). Altogether, these data emphasize an important role of CD63 in intrinsically preserving HSC function.

CD63 deficiency impairs TGFβ signaling in HSCs

As we know, TGFβ signaling is essential for maintaining the quiescence of HSCs [15, 44]. Interestingly, further analysis of the RNA-seq data showed that CD63 expression was correlated with TGFβ signaling activity in HSCs (Fig. 6A). Consistently, the phosphorylation level of Samd2/3, a specific indicator of TGFβ signaling [45], was higher in $CD63^{hi}$ HSCs than in $CD63^{-/lo}$ HSCs, although the expression of TGFβ receptors I and II was comparable (Fig. 6B and Supplementary Fig. S7A, B). Alternatively, CD63 expression was higher in p-$Smad2/3^{hi}$ HSCs than in p-$Smad2/3^{-/lo}$ HSCs (Fig. 6C). These findings led us to examine whether CD63 regulates TGFβ signaling in HSCs. Indeed, Smad2/3 phosphorylation was significantly decreased in HSCs when CD63 was deleted (Fig. 6D), which was not caused by the reduced expression of TGFβ receptors I and II in HSCs, as well as a decreased level of TGFβ1 in the BM (Fig. 6E–G). Furthermore, impaired TGFβ signaling in CD63-null HSCs was confirmed by Western blot and immunofluorescence analyses (Fig. 6H, I). In accordance with these data, the level of p57, a direct target gene of TGFβ signaling [44, 46], was markedly decreased (Fig. 6J). Additionally, p21 and c-myc, which are respectively activated and inhibited by TGFβ signaling [45], were correspondingly downregulated and upregulated in HSCs in the absence of CD63 (Fig. 6J). Previous studies indicated that tetraspanins function as interacting webs [47]. However, it was found that loss of CD63 did not significantly affect the expression of other common tetraspanins, including CD9, CD37, CD53, CD81, CD82, and CD151, in HSCs (Supplementary Fig. S7C–H). Hence, these data elucidate that CD63 may be required to sustain TGFβ signaling in HSCs.

CD63 regulates TGFβ signaling by interacting with TGFβ receptors I and II

After binding to TGFβ1, TGFβ receptor II recruits and phosphorylates TGFβ receptor I, which then activates downstream signaling molecules [15, 48]. Notably, we noticed that the interaction between TGFβ receptor II and TGFβ receptor I was decreased after CD63 knockout (Fig. 7A, B). Consistently, CD63 deficiency resulted in a significant decrease in the colocalization of TGFβ receptor I to TGFβ receptor II in HSCs by immunofluorescence analysis (Supplementary Fig. S8A). Combining these findings with previous reports that CD63 can interact with several receptors on the cell surface, we speculated that CD63 may be involved in regulating TGFβ signaling activity by associating with TGFβ receptors. As expected, co-immunoprecipitation (Co-IP) assay confirmed that CD63 can interact with TGFβ receptors I and II under physiological conditions (Fig. 7C, D). Immunofluorescence analysis revealed that a large portion of CD63 was colocalized to TGFβ receptors I (Pearson's correlation coefficient: 0.839 ± 0.081) and II (Pearson's correlation coefficient: 0.821 ± 0.076) in HSCs (Fig. 7E, F), further consolidating this finding. To further determine whether CD63 is needed for the activation of TGFβ signaling, we purified WT and $CD63^{-/-}$ HSCs and treated them with recombinant TGFβ1 in vitro. In agreement with the results of previous studies [44, 49], Smad2/3 was rapidly dephosphorylated in HSCs from WT mice by in vitro cytokine stimulation, whereas its remained phosphorylated when pretreated with TGFβ1 (Fig. 7G). In contrast, $CD63^{-/-}$ HSCs were insensitive to TGFβ1 stimulation in vitro (Fig. 7G). Finally, we found that overexpression of CD63 restored TGFβ signaling activity and rescued the defective quiescence and engraftment potential of CD63-null HSCs (Fig. 7H–J and Supplementary Fig. S8B). Collectively, these findings demonstrate that CD63-mediated regulation of TGFβ signaling plays a crucial role in the maintenance of HSC quiescence (Fig. 7K).

DISCUSSION

Life-long hematopoiesis is supported by HSCs with great self-renewal ability to allow continuous production of hematopoietic progenitors and various mature blood cells [50, 51]. Although the

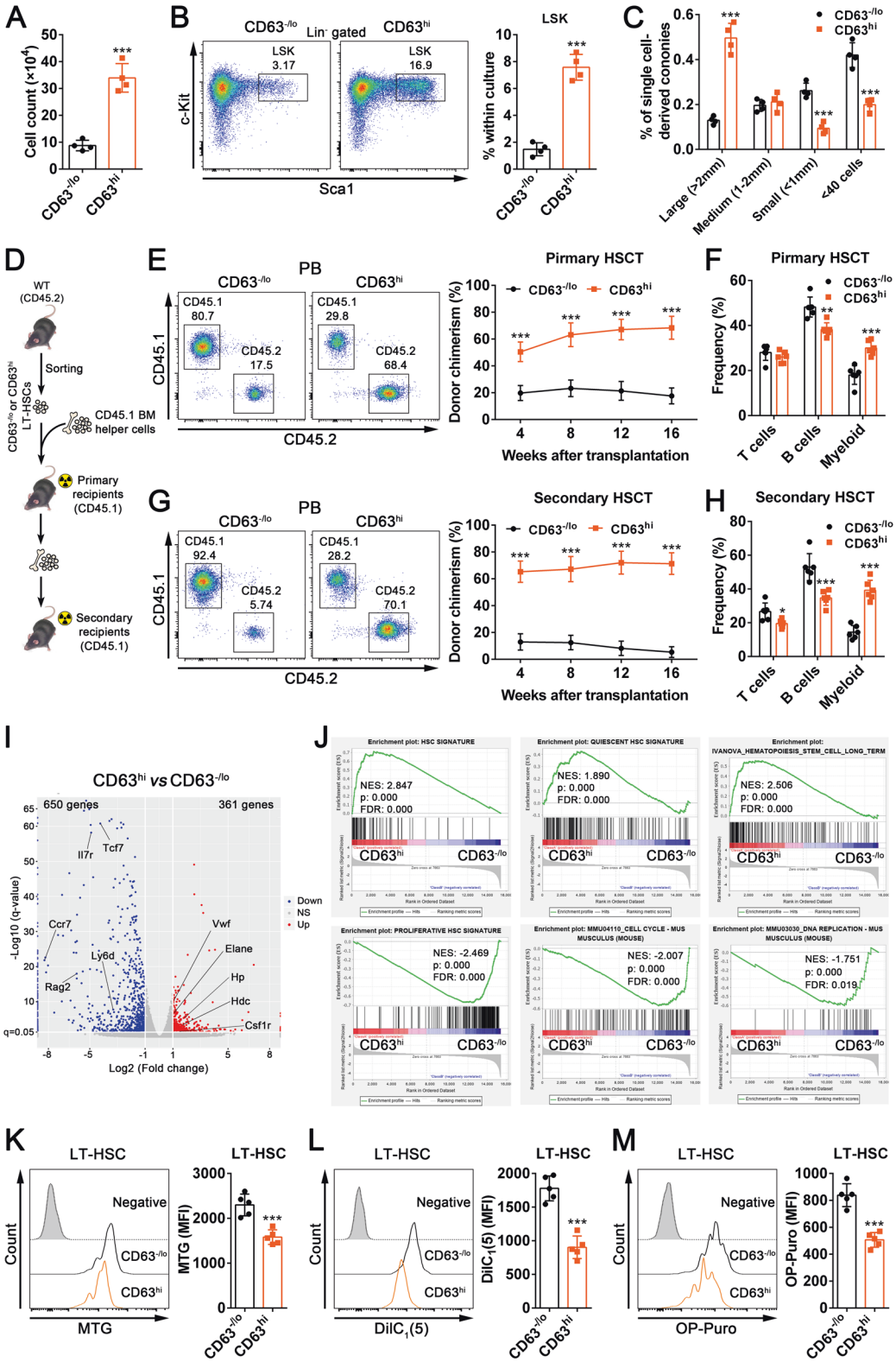

factors involved in hematopoietic modulation have been widely studied, how to precisely regulate the behavior of HSCs is still unknown. In addition, HSC populations have been recognized to be highly heterogeneous [9, 11]. Therefore, further examination of reliable markers may help us to obtain a deep understanding of the biological characteristics of HSCs. In this report, we demonstrate for the first time that CD63 is a functional marker of HSCs and maintains the quiescence of HSCs by supporting TGFβ signaling through interaction with TGFβ receptors I and II.

In most cell types, the majority of CD63 is present at lysosome-associated membranes rather than the plasma membrane [23]. Hence, CD63 is also called lysosome-associated membrane protein 3 (LAMP-3) [29]. In the present study, by comparing surface staining with intracellular staining, we observed that CD63 is

Fig. 2 CD63^{hi} LT-HSCs display more robust self-renewal and myeloid differentiation ability. A, **B** 1×10^3 CD63$^{-/lo}$ and CD63^{hi} LT-HSCs sorted from the BM of normal mice were cultured in liquid medium for 10 days. **A** The total cell numbers in culture were counted ($n = 4$). Data are shown as the mean ± SD. ***$P < 0.001$. **B** The percentage of LSKs in culture was detected by flow cytometry ($n = 4$). Representative flow cytometric plots are shown in the left. Data are shown as the mean ± SD. ***$P < 0.001$. **C** Single CD63$^{-/lo}$ and CD63^{hi} LT-HSC sorted from the BM of normal mice were cultured in methylcellulose medium for 14 days. The size distribution of 240 single-cell is shown ($n = 4$). Data are shown as the mean ± SD. ***$P < 0.001$. **D**–**H** 3×10^2 CD63$^{-/lo}$ and CD63^{hi} LT-HSCs, along with 5×10^5 CD45.1 BM helper cells, were transplanted into lethally irradiated CD45.1 mice. Sixteen weeks later, 1×10^6 BM cells from the primary recipient mice were transplanted into secondary CD45.1 recipient mice. **D** The strategy for HSC transplantation (HSCT). **E**, **G** The percentage of donor-derived cells in the peripheral blood (PB) of (**E**) primary and (**G**) secondary recipients was measured at the indicated time by flow cytometry ($n = 6$). Representative flow cytometric plots of 16 weeks after primary and secondary transplantation are shown in the left. Data are shown as the mean ± SD. ***$P < 0.001$. **F**, **H** The lineage distribution of donor-derived cells in the PB of (**F**) primary and (**H**) secondary recipients at 16 weeks after transplantation was determined by flow cytometry ($n = 6$). Data are shown as the mean ± SD. *$P < 0.05$, **$P < 0.01$, ***$P < 0.001$. **I**, **J** CD63$^{-/lo}$ and CD63^{hi} LT-HSCs sorted from the BM of normal mice were subjected to RNA-seq analysis ($n = 3$). **I** Volcano plot showing the differentially expressed genes (DEGs) between CD63$^{-/lo}$ and CD63^{hi} LT-HSCs. DEGs were identified using the combined criteria |log2 fold change| > 1 and q-value < 0.05. Representative myeloid- and lymphoid-specific DEGs are indicated. **J** Gene set enrichment analysis (GSEA) of the RNA-seq data. GSEA plots of HSC signature, quiescence, long-term, proliferation, cell cycle, and DNA duplication are shown. NES, normalized enrichment scores; FDR, false discovery rates. **K** Flow cytometric analysis of mitochondrial mass in CD63$^{-/lo}$ and CD63^{hi} LT-HSCs from the BM of normal mice by MitoTracker Green (MTG) staining ($n = 5$). Representative flow cytometric plots are shown in the left. Data are shown as the mean ± SD. ***$P < 0.001$. **L** Flow cytometric analysis of mitochondrial membrane potential in CD63$^{-/lo}$ and CD63^{hi} LT-HSCs from the BM of normal mice by DiIC$_1$(5) staining ($n = 5$). Representative flow cytometric plots are shown in the left. Data are shown as the mean ± SD. ***$P < 0.001$. **M** Flow cytometric analysis of O-propargyl-puromycin (OP-Puro) incorporation in CD63$^{-/lo}$ and CD63^{hi} LT-HSCs from the BM of normal mice ($n = 5$). Representative flow cytometric plots are shown in the left. Data are shown as the mean ± SD. ***$P < 0.001$.

abundantly expressed on the cell surface in HSPCs. Although CD63 expression was higher in LT-HSCs than in other progenitor cells, its distribution in this population was still inhomogeneous. We therefore subfractionated phenotypic HSCs into two fractions based on the level of CD63 and found that the fractions had different characteristics. CD63^{hi} HSCs were more quiescent and displayed a more robust ability in self-renewal. Meantime, CD63^{hi} HSCs were biased toward myeloid differentiation, which is consistent with the observation that myeloid-biased HSCs exhibit more quiescent property and stronger reconstitution potential than lymphoid-biased HSCs [18, 21, 52]. As a consequence, our data show that CD63, in combination with conventional markers, may be used to identify more primitive HSCs in mice. In contrast, a previous study reported that CD63 expression is lower in more primitive human CD34$^+$ CD133$^+$ cells than the relatively mature CD34$^+$ CD133$^{low/-}$ cells [28], which suggests that discrepancies with respect to HSPC markers may exist between distinct species. In fact, many surface markers, such as CD9, CD34, CD48, and CD150, display different expression patterns between mouse and human HSCs [47, 53, 54].

At the cell surface, tetraspanins form membrane microdomains called tetraspanin-enriched microdomains (TEMs) with a variety of proteins, such as integrins, receptors, and other membrane-bound proteins [55]. These structures are defined as novel signaling platforms functionally different from lipid rafts and are usually cell-type specific [25]. A growing body of research shows that cell surface CD63 expression is crucial for its function within TEMs [56, 57]. Although CD63 has been extensively explored in multiple hematopoietic and immune cells, including macrophages, neutrophils, dendritic cells, mast cells, and platelets [23, 24, 27], little is known about its potential role in HSCs. Here, we found that CD63 deficiency decreased the number and quiescence of HSCs in mice. In steady-state BM, most HSCs, especially LT-HSCs, are retained in a highly quiescent or dormant state, which is a critical property responsible for protecting them from injuries caused by irradiation and cytotoxic substances and keeping their long-term repopulating ability [7, 58]. Expectedly, we found that CD63$^{-/-}$ mice were highly sensitive to TBI and 5-FU treatment. On the other hand, to functionally characterize the role of CD63 in HSCs, we then performed a series of transplantation assays. It was observed that deletion of CD63 dramatically impaired the long-term repopulating ability of HSCs in a cell-intrinsic manner. Collectively, these data indicate that CD63 is required to guard the quiescence and engraftment potential of HSCs.

It is well accepted that the TGFβ signaling pathway is indispensable for the maintenance of HSC quiescence [3]. Although TGFβ signaling in HSCs can be independently regulated by several factors, including Tif1, Msi2, ESL-1, SHP-1, and miR-143/145 [46, 48, 49, 59, 60], the underlying regulatory mechanism has not been completely uncovered. In this work, we found that TGFβ signaling is significantly decreased in HSCs in the absence of CD63, in accordance with data showing that HSCs with high expression of CD63 display higher TGFβ signaling activity. After TGFβ receptor II binds to its ligand, its recruitment to TGFβ receptor I is a key step in initiating this signaling pathway [15]. Importantly, we found that there was evident attenuation of the binding of TGFβ receptor II to TGFβ receptor I after CD63 knockout, accompanied by a decreased level of p-Smad2/3. Subsequent Co-IP and immunofluorescence assays showed that CD63 can directly or indirectly interact with TGFβ receptors I and II. In this context, we speculated that CD63 may interact with TGFβ receptors I and II and then promote their binding, thereby maintaining the quiescence of HSCs. Furthermore, we noted that the percentage of donor-derived myeloid cells was significantly reduced in secondary recipients transplanted with CD63-null HSCs, which is consistent with the finding that TGFβ signaling facilitates myeloid-biased differentiation of HSCs [59]. In addition, our findings may explain why myeloid-biased and lymphoid-biased HSCs respond differently to TGFβ1 stimulation [18].

On the other hand, CD63 can function as a mediator of its interaction protein adaptor protein complex-2 (AP-2) to promote clathrin-mediated endocytosis of the protein complex [27]. As a previous study reported, CD63 modulates intracellular transport of its interaction partners in some specific cell types, such as antigen-presenting cells and gastric parietal cells [23]. However, we did not find any difference in the expression of TGFβ receptors I and II between WT and CD63$^{-/-}$ HSCs, suggesting that the impaired TGFβ signaling in HSCs after CD63 knockout is not due to abnormal transport of TGFβ receptors. Additionally, we cannot exclude the possibility that CD63 may be involved in regulating other signaling pathways, such as the tissue inhibitor of metalloproteinase-1 (TIMP-1)-mediated pathway [61], in mouse HSCs. Therefore, further research is still needed.

In conclusion, these data identify CD63 as a previously unknown marker that distinguishes distinct HSC subpopulations in mice. Moreover, we demonstrate that CD63 supports TGFβ signaling through association with TGFβ receptors I and II, an event that is required to maintain HSC quiescence, thus deepening our understanding of the physiological function of CD63.

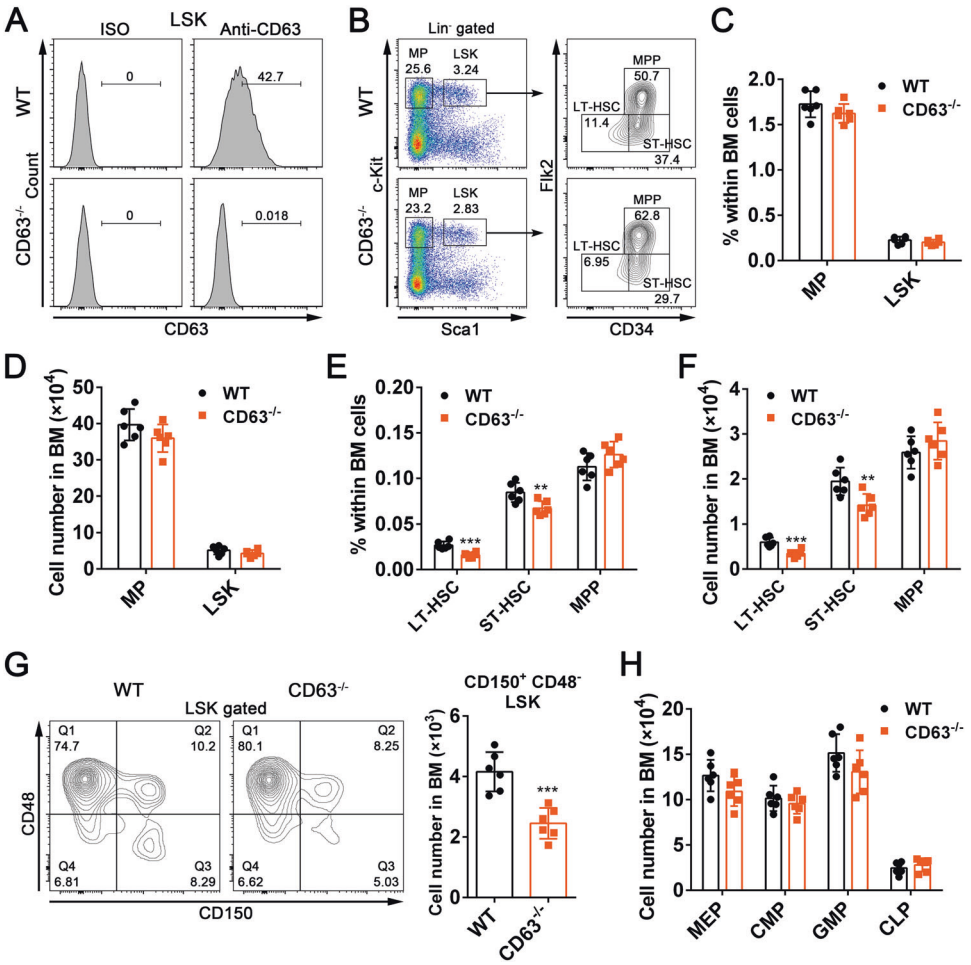

Fig. 3 Knockout of CD63 results in a reduced number of HSCs in mice. A Flow cytometric analysis of cell surface expression of CD63 in LSKs from the BM of WT and CD63$^{-/-}$ mice. Representative flow cytometric plots of four biological replicates are shown. **B** Representative flow cytometric plots showing the percentage of HSPCs in the BM of WT and CD63$^{-/-}$ mice. **C**, **D** The (**C**) percentages and (**D**) absolute numbers (one leg) of LSKs and MPs in the BM of WT and CD63$^{-/-}$ mice ($n = 6$). Data are shown as the mean ± SD. **E**, **F** The (**E**) percentages and (**F**) absolute numbers (one leg) of LT-HSCs, ST-HSCs, and MPPs in the BM of WT and CD63$^{-/-}$ mice ($n = 6$). Data are shown as the mean ± SD. $^{**}P < 0.01$, $^{***}P < 0.001$. **G** The absolute number (one leg) of CD150^{+} CD48^{-} LSKs in the BM of WT and CD63$^{-/-}$ mice ($n = 6$). Representative flow cytometric plots are shown in the left. Data are shown as the mean ± SD. $^{***}P < 0.001$. **H** The absolute numbers (one leg) of granulocyte monocyte progenitors (GMPs; Lin^{-} c-Kit^{+} Sca1^{-} CD127^{-} CD16/32^{+} CD34^{+}), common myeloid progenitors (CMPs; Lin^{-} c-Kit^{+} Sca1^{-} CD127^{-} CD16/32^{-} CD34^{+}), megakaryocyte erythroid progenitors (MEPs; Lin^{-} c-Kit^{+} Sca1^{-} CD127^{-} CD16/32^{-} CD34^{-}) and common lymphoid progenitors (CLPs; Lin^{-} CD127^{+} c-Kit^{low} Sca1^{low}) in the BM of WT and CD63$^{-/-}$ mice ($n = 6$). Data are shown as the mean ± SD.

MATERIALS AND METHODS

Animals

CD63$^{-/-}$ mice (C57BL/6J background) were purchased from Model Organisms Center (Shanghai, China), and their WT littermates were used as controls. Congenic CD45.1 mice were a gift from Prof. Jinyong Wang (Guangzhou Institutes of Biomedicine and Health, Chinese Academy of Science, Guangzhou, China). Normal WT C57BL/6J mice were obtained from the Institute of Zoology (Chinese Academy of Sciences, Beijing, China). All mice were housed in a specific pathogen-free facility (The Third Military Medical University, Chongqing, China). Unless otherwise stated, the mice used were male and 6–8 weeks old. When treatment was used, mice were randomly assigned to each group. No blinding was performed in this study. The sample size was determined by extensive experience, and no mice or samples were excluded. Animal experiments were performed according to the guidelines approved by the Animal Care Committee of The Third Military Medical University.

Flow cytometry

BM cells were flushed from the femora and tibiae of mice, and single-cell suspensions were then prepared as we previously reported. The following anti-mouse antibodies obtained from eBioscience (San Diego, CA, USA), Biolegend (San Diego, CA, USA), BD Biosciences (San Jose, CA, USA) or R&D Systems (Minneapolis, MN, USA) were used for flow cytometric analysis or sorting: anti-Lineage antibody cocktail (containing CD3e, Mac-1, Gr-1, B220 and Ter-119), anti-c-Kit, anti-Sca-1, anti-Flk2 (CD135), anti-CD34, anti-CD48, anti-CD150, anti-CD16/32, anti-CD127, anti-CD3e, anti-B220, anti-Mac-1 (CD11b), anti-Gr-1, anti-CD45.1, anti-CD45.2, anti-CD63, anti-CD9, anti-CD37, anti-CD53, anti-CD81, anti-CD82, anti-CD151, anti-Annexin V, anti-Ki67, anti-p-Smad2/3, anti-TβRI, anti-TβRII, anti-γ-H2AX^{S139} and anti-p-Smad2$^{S465/S467}$/Smad3$^{S423/S425}$. The details of the antibodies are provided in Supplementary Table S1.

Cell cycle analysis, apoptosis analysis, γ-H2AX staining, intracellular protein staining, in vivo BrdU incorporation assay and mitochondrial activity detection were carried out as we previously described [62, 63]. Cells were detected using a FACSVerse or FACSCanto flow cytometer (BD Biosciences) and sorted using a FACSAria II cell sorter (BD Biosciences). All data were analyzed with FlowJo 10.0 software (TreeStar, San Carlos, CA, USA).

Protein synthesis assay

The in vivo protein synthesis rate was measured as previously reported [64]. Briefly, mice were intraperitoneally injected with O-propargyl-puromycin

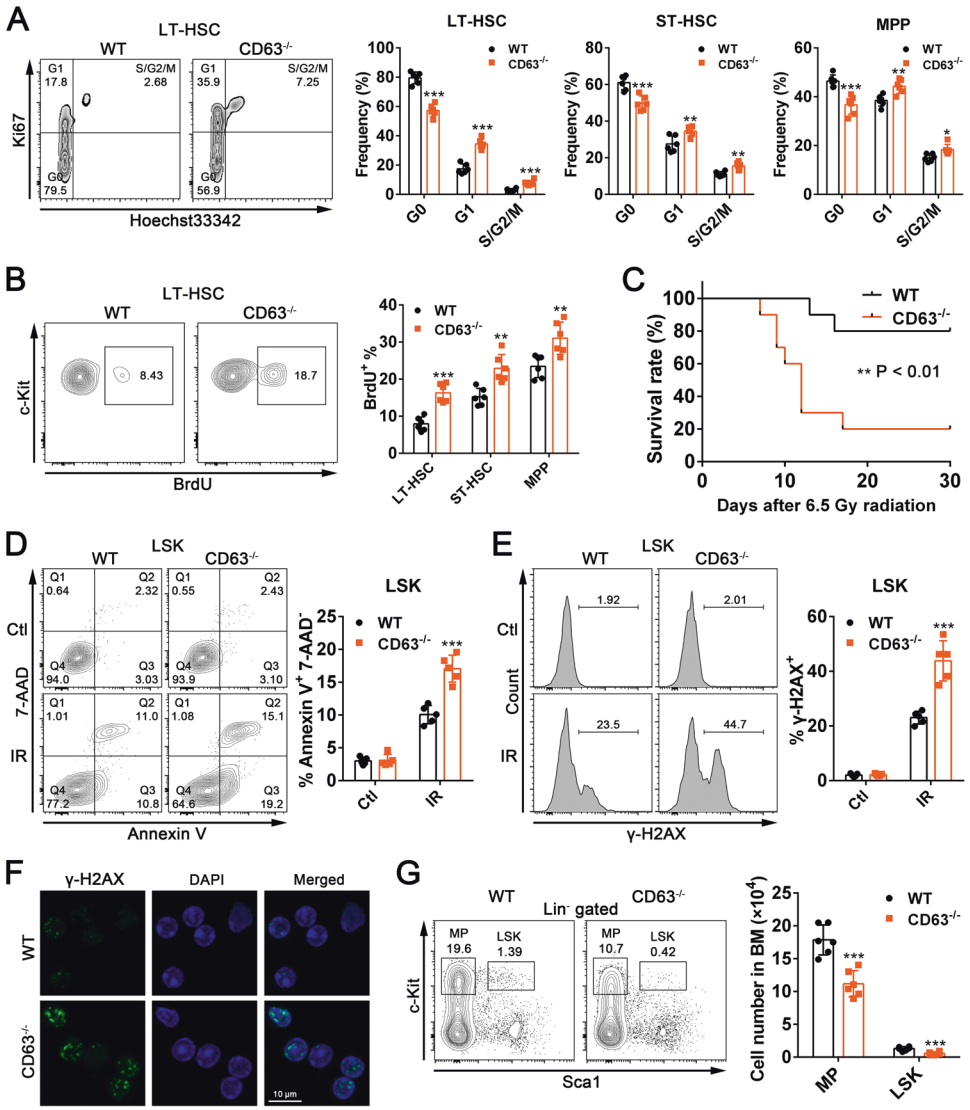

Fig. 4 Deletion of CD63 leads to impairment of HSC quiescence. A Flow cytometric analysis of the cell cycle status of LT-HSCs, ST-HSCs and MPPs from the BM of WT and CD63$^{-/-}$ mice ($n = 6$). Representative flow cytometric plots for LT-HSCs are shown in the left. Data are shown as the mean ± SD. *$P < 0.05$, **$P < 0.01$, ***$P < 0.001$. **(B)** Flow cytometric analysis of the in vivo BrdU incorporation of LT-HSCs, ST-HSCs, and MPPs from the BM of WT and CD63$^{-/-}$ mice ($n = 6$). Representative flow cytometric plots for LT-HSCs are shown in the left. Data are shown as the mean ± SD. **$P < 0.01$, ***$P < 0.001$. **C** The survival rates of WT and CD63$^{-/-}$ mice after a single dose of 6.5 Gy TBI ($n = 10$). Kaplan–Meier survival curves and log-rank test were used to analyze the survival rates of mice. **$P < 0.01$. **D** Flow cytometric analysis of the apoptosis of LSKs from the BM of WT and CD63$^{-/-}$ mice during steady-state or 12 h after a single dose of 6.0 Gy TBI ($n = 5$). Representative flow cytometric plots are shown in the left. Data are shown as the mean ± SD. ***$P < 0.001$. Ctl, control; IR, irradiation. **E** Flow cytometric analysis of γ-H2AX^{S139} expression in LSKs from the BM of WT and CD63$^{-/-}$ mice during steady-state or 2 h after a single dose of 2.0 Gy TBI ($n = 5$). Data are shown as the mean ± SD. ***$P < 0.001$. **F** Immunofluorescence analysis of γ-H2AX^{S139} expression in LSKs freshly sorted from the BM of WT and CD63$^{-/-}$ mice 2 h after a single dose of 2.0 Gy TBI. Representative immunofluorescence images of three biological replicates are shown. The scale bar indicates 10 μm. **G** The absolute numbers (one leg) of LSKs and MPs in the BM of WT and CD63$^{-/-}$ mice 15 days after 5.0 Gy TBI ($n = 6$). Representative flow cytometric plots are shown in the left. Data are shown as the mean ± SD. ***$P < 0.001$.

(OP-Puro) (50 mg/kg). One hour later, BM cells were collected and stained with HSPC surface markers. Finally, the incorporation of OP-Puro was detected using a Click-iT Plus OPP Protein Synthesis Assay Kit (Molecular Probes, Carlsbad, CA, USA).

HSC culture and single LT-HSC colony-formation assay

Freshly sorted HSCs were cultured in StemSpan SFEM (Stem Cell Technologies, Grenoble, France) containing SCF (10 ng/ml; PeproTech, Rocky Hill, NJ, USA), TPO (20 ng/ml; PeproTech), heparin (10 μg/ml; MedChemExpress, Princeton, NJ, USA) and penicillin/streptomycin (1%; Sigma, St. Louis, MO, USA). After 10 days of culture, cells were counted and analyzed by flow cytometry. A single LT-HSC colony-formation assay was performed using methylcellulose medium (M3434; Stem Cell Technologies) as we described previously [62].

In vitro treatment with TGFβ1

In vitro TGFβ1 treatment was conducted as reported [44]. Briefly, LT-HSCs were sorted in StemSpan SFEM with or without TGFβ1 (5 ng/ml; PeproTech) and incubated at 37 °C for 30 min. Then, cells were stimulated with SCF (50 ng/ml) and TPO (50 ng/ml) and incubated at 37 °C for another 30 min, followed by immunofluorescence analysis.

Transplantation assays

For competitive BM transplantation assay, 5×10^5 BM cells from WT and CD63$^{-/-}$ mice were mixed with CD45.1 mice BM cells at a ratio of 1:1 and were then transplanted into lethally irradiated (10.0 Gy) CD45.1 mice via tail intravenous injection. Sixteen weeks later, 1×10^6 BM cells from the primary recipient mice were transplanted into secondary CD45.1 recipient

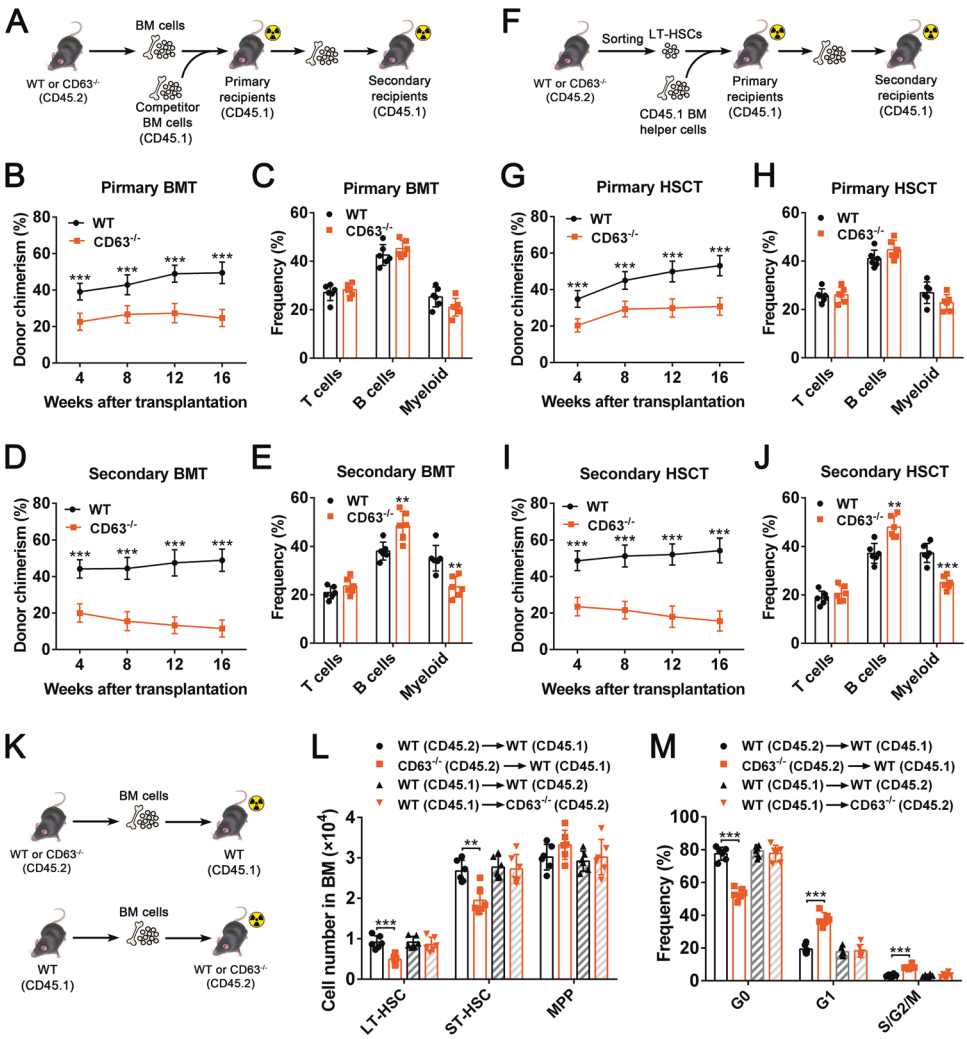

Fig. 5 Loss of CD63 compromises the long-term repopulating ability of HSCs. A–E 5×10^5 BM cells from WT or CD63$^{-/-}$ mice (CD45.2) were mixed with CD45.1 competitive BM cells (at the ratio of 1:1) and then were transplanted into lethally irradiated CD45.1 mice. Sixteen weeks later, 1×10^6 BM cells from the primary recipient mice were transplanted into secondary CD45.1 recipient mice. **A** The strategy for competitive BM transplantation (BMT). **B**, **D** The percentage of donor-derived cells in the PB of (**B**) primary and (**D**) secondary recipients was measured at the indicated time by flow cytometry ($n = 6$). Data are shown as the mean ± SD. ***$P < 0.001$. **C**, **E** The lineage distribution of donor-derived cells in the PB of (**C**) primary and (**E**) secondary recipients at 16 weeks after transplantation was determined by flow cytometry ($n = 6$). Data are shown as the mean ± SD. **$P < 0.01$. **F–J** 3×10^2 WT or CD63$^{-/-}$ LT-HSCs (CD45.2), along with 5×10^5 CD45.1 BM helper cells, were transplanted into lethally irradiated CD45.1 mice. Sixteen weeks later, 1×10^6 BM cells from the primary recipient mice were transplanted into secondary CD45.1 recipient mice. **F** The strategy for HSC transplantation (HSCT). **G**, **I** The percentage of donor-derived cells in the PB of (**G**) primary and (**I**) secondary recipients was measured at the indicated time by flow cytometry ($n = 6$). Data are shown as the mean ± SD. ***$P < 0.001$. **H**, **J** The lineage distribution of donor-derived cells in the PB of (**H**) primary and (**J**) secondary recipients at 16 weeks after transplantation was determined by flow cytometry ($n = 6$). Data are shown as the mean ± SD. **$P < 0.01$, ***$P < 0.001$. **K–M** 1×10^6 BM cells from WT or CD63$^{-/-}$ mice (CD45.2) were transplanted into lethally irradiated WT mice (CD45.1). Meanwhile, 1×10^6 BM cells from WT mice (CD45.1) were transplanted into lethally irradiated WT or CD63$^{-/-}$ mice (CD45.2). Sixteen weeks later, recipient mice were used for subsequent analysis. **K** The strategy for reciprocal BMT. **L** The absolute numbers of LT-HSCs, ST-HSCs, and MPPs in the BM (one leg) of recipient mice ($n = 6$). Data are shown as the mean ± SD. **$P < 0.01$, ***$P < 0.001$. **M** The cell cycle status of LT-HSCs in the BM of recipient mice ($n = 6$). Data are shown as the mean ± SD. ***$P < 0.001$.

mice. For HSC transplantation assays, 3×10^2 CD63$^{-/lo}$ and CD63^{hi} LT-HSCs from normal WT mice or 3×10^2 LT-HSCs from WT and CD63$^{-/-}$ mice were transplanted intravenously along with 5×10^5 CD45.1 BM helper cells into lethally irradiated CD45.1 recipient mice. Sixteen weeks later, 1×10^6 BM cells from the primary recipient mice were transplanted into secondary CD45.1 recipient mice. For the rescue experiment, 5×10^3 WT or CD63$^{-/-}$ LSKs transduced with lentivirus carrying CD63 or control vectors, together with 5×10^5 CD45.1 BM helper cells, were transplanted into lethally irradiated CD45.1 recipient mice. Reciprocal transplantation and homing assays were conducted as we previously described [62]. Donor engraftment and lineage distribution were measured at the indicated times after transplantation.

Lentiviral transduction

The lentivirus carrying CD63 gene or control vectors were constructed at Hanbio Co. Ltd. (Shanghai, China). Mouse LSKs were transduced with the recombinant lentivirus as we previously reported [62]. Transduced cells (GFP$^+$) were sorted by flow cytometry and were then used for immunofluorescence analysis or transplantation assays.

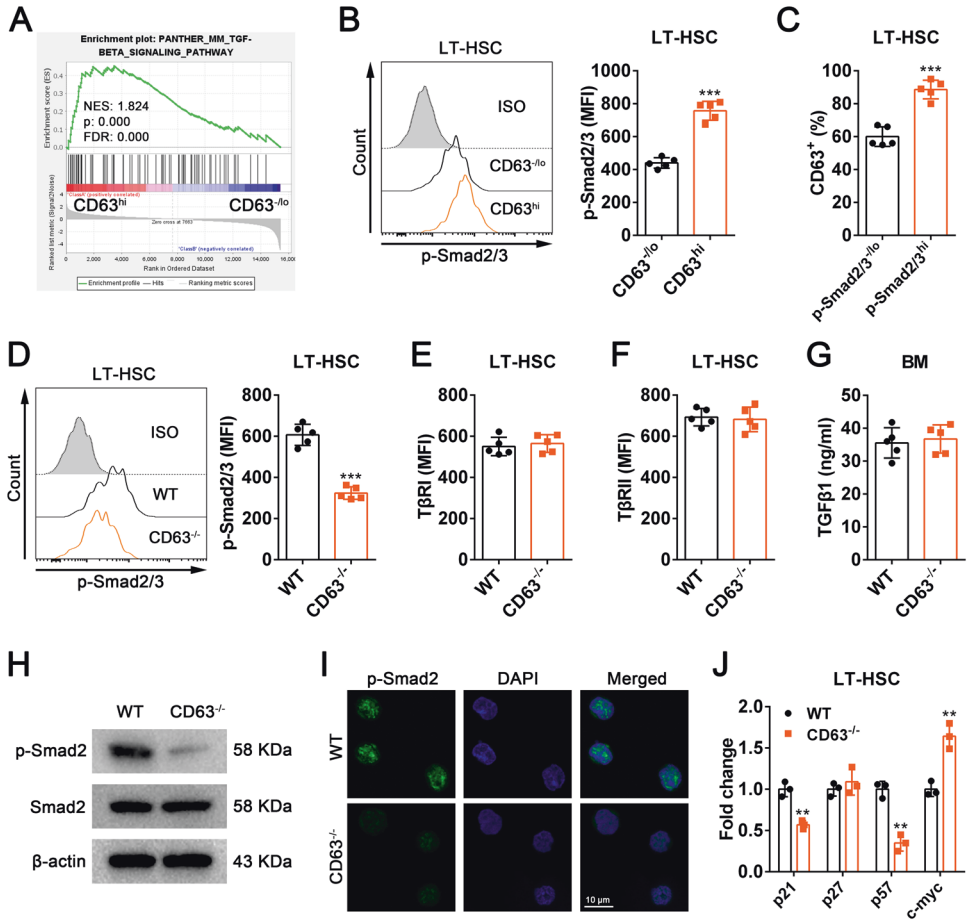

Fig. 6 CD63 deficiency impairs TGFβ signaling in HSCs. A GSEA of the RNA-seq data from CD63$^{-/lo}$ and CD63^{hi} LT-HSCs. GSEA plot of TGFβ signaling pathway is shown. **B** Flow cytometric analysis of p-Smad2$^{S465/S467}$/Smad3$^{S423/S425}$ expression in CD63$^{-/lo}$ and CD63^{hi} LT-HSCs from the BM of normal mice ($n = 5$). Representative flow cytometric plots are shown in the left. Data are shown as the mean ± SD. ***$P < 0.001$. **C** Flow cytometric analysis of CD63 expression in p-Smad2/3$^{-/low}$ (p-Smad2/3$^{-/lo}$) and p-Smad2/3^{high} (p-Smad2/3^{hi}) LT-HSCs from the BM of normal mice ($n = 5$). LT-HSCs were divided into p-Smad2/3^{-lo} (down 30%) and p-Smad2/3^{hi} (up 30%) fractions based on the expression of p-Smad2/3. Data are shown as the mean ± SD. ***$P < 0.001$. **D** Flow cytometric analysis of p-Smad2$^{S465/S467}$/Smad3$^{S423/S425}$ expression in LT-HSCs from the BM of WT and CD63$^{-/-}$ mice ($n = 5$). Representative flow cytometric plots are shown in the left. Data are shown as the mean ± SD. ***$P < 0.001$. **E**, **F** Flow cytometric analysis of (**E**) TβRI and (**F**) TβRII expression in LT-HSCs from the BM of WT and CD63$^{-/-}$ mice ($n = 5$). Data are shown as the mean ± SD. TβRI, TGFβ receptor I; TβRII, TGFβ receptor II. **G** Enzyme linked immunosorbent assay (ELISA) analysis of TGFβ1 level in the BM of WT and CD63$^{-/-}$ mice ($n = 5$). Data are shown as the mean ± SD. **H** Western blot analysis of p-Smad2$^{S465/S467}$ expression in LSKs freshly sorted from the BM of WT and CD63$^{-/-}$ mice. Representative Western blot plots of three biological replicates are shown. **I** Immunofluorescence analysis of p-Smad2$^{S465/S467}$ expression in LT-HSCs freshly sorted from the BM of WT and CD63$^{-/-}$ mice. Representative immunofluorescence images of three biological replicates are shown. The scale bar indicates 10 μm. **J** qRT-PCR analysis of the expression of p21, p27, p57, and c-myc in LT-HSCs freshly sorted from the BM of WT and CD63$^{-/-}$ mice ($n = 3$). Data are shown as the mean ± SD. **$P < 0.01$.

Quantitative RT-PCR (qRT-PCR)

This assay was performed as we previously described [63, 65]. The primer sequences are listed in Supplementary Table S2.

RNA-seq

Total RNA from freshly sorted CD63$^{-/lo}$ and CD63^{hi} LT-HSCs was extracted using an RNAqueous kit (Ambion, Darmstadt, Germany). RNA-seq was carried out at Sinotech Genomics Inc. (Shanghai, China). Differentially expressed genes were identified using the combined criteria |log2 fold change| > 1 and q-value < 0.05. GSEA was performed using GSEA version 4.0.3 (http://www.broadinstitute.org/gsea), and gene sets were obtained from MSigDB (http://www.broadinstitute.org/gsea/msigdb) or a previous study [66]. All raw data were deposited in the NCBI Sequence Read Archive (SRA) database (no. PRJNA698278).

scRNA-seq

The scRNA-seq data were obtained from the Gene Expression Omnibus (GEO accession number: GSE90742) database and analyzed using Seurat v3.1.1 (https://satijalab.org/seurat/archive/v3.1/pbmc3k_tutorial.html). Data from low-quality cells were excluded based on the following criteria: (1) genes detected in < 3 cells; (2) cells with < 200 total detected genes; and (3) cells with ≥ 10% mitochondrially encoded genes. The remaining 4785 cells in all fractions of LT-HSCs, MPP1, MPP2, MPP3, and MPP4 were normalized to reproduce the previously reported results as faithfully as possible [30], while genes associated with the cell cycle were not included. PCA was performed to identify significantly available dimensions via elbow plots. Then, the t-distributed stochastic neighbor embedding (t-SNE) algorithm was applied for dimensionality reduction with 13 initial principal components. All cells were grouped into 11 clusters by the unsupervised clustering method and sorted using surface markers described previously [30].

Western blot

This analysis was performed as we previously described [62]. The details of the antibodies are provided in Supplementary Table S1.

Co-IP

Lin$^-$ cells freshly sorted from mouse BM were lysed in IP cell lysis buffer. Immunoprecipitation was carried out using a Dynabeads™ Protein G

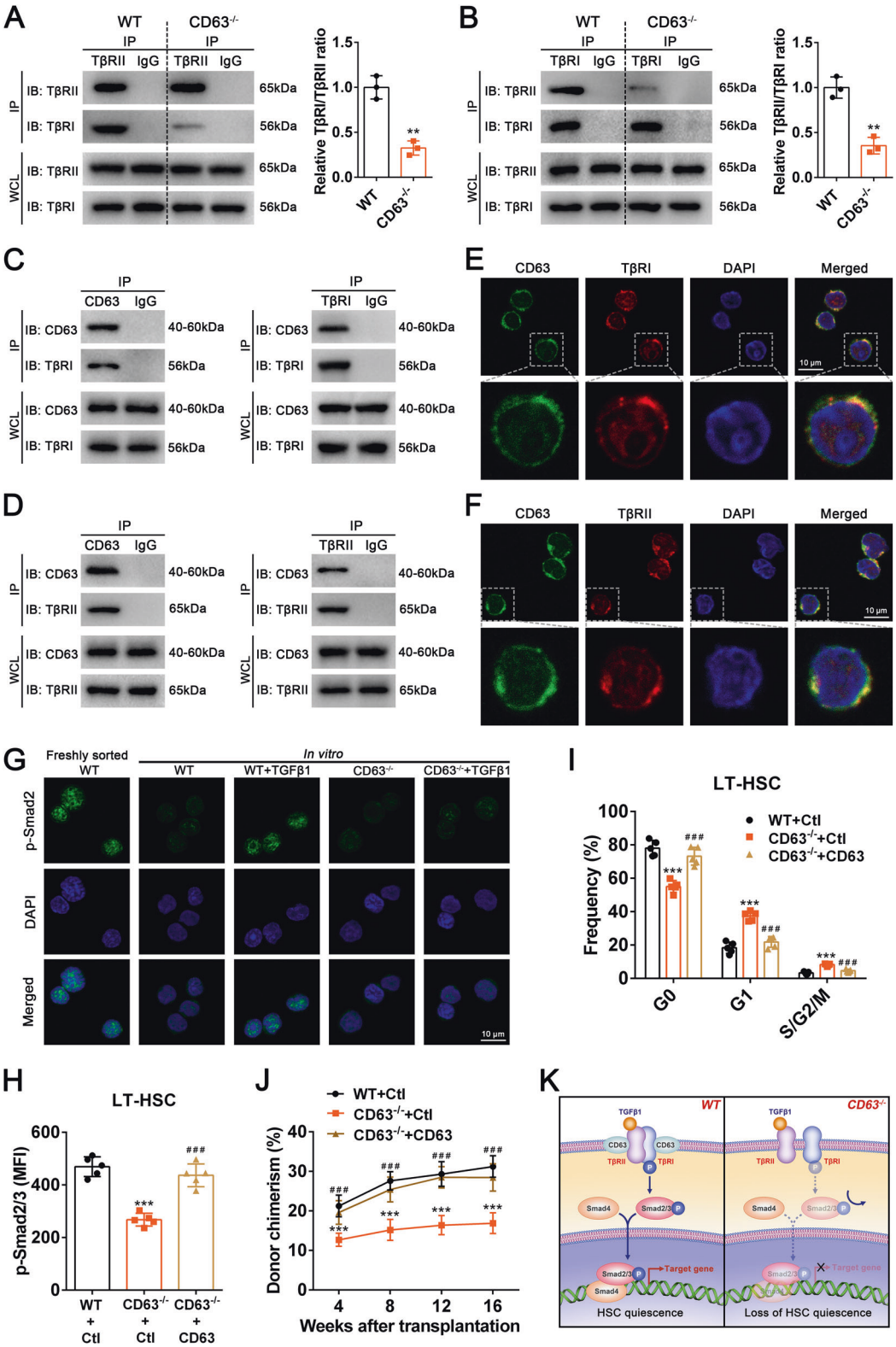

Immunoprecipitation Kit (Invitrogen, Carlsbad, CA, USA) as we described previously [67]. Then, immunoprecipitated proteins were subjected to Western blot analysis. To avoid interference from IgG heavy chain or light chain, the antibodies used for immunoprecipitation and Western blot analysis were raised in different host species. Quantification of bands was performed using Fiji software (National Institutes of Health, Bethesda, MD, USA). The details of the antibodies are provided in Supplementary Table S1.

Immunofluorescence

Sorted HSCs were placed on poly-L-lysine coating slides. Then, cells were fixed with 4% paraformaldehyde and permeabilized with 0.5% Triton

Fig. 7 CD63 regulates TGFβ signaling by interacting with TGFβ receptors I and II. A, **B** Co-immunoprecipitation (Co-IP) analysis of the interaction of TβRI and TβRII in Lin^- cells freshly sorted from the BM of WT and $CD63^{-/-}$ mice. The whole-cell lysates (WCL) were used as input and loading control. Representative immunoblotting (IB) plots of three biological replicates are shown in the left. Quantitation analysis of (**A**) relative TβRI/TβRII or (**B**) TβRII/TβRI ratio is shown in the right. Data are shown as the mean ± SD. $^{**}P < 0.01$. **C**, **D** Co-IP analysis of the interaction between CD63 and (**C**) TβRI or (**D**) TβRII in Lin^- cells freshly sorted from the BM of normal mice. The whole-cell lysates (WCL) were used as input and loading control. Representative IB plots of three biological replicates are shown. **E**, **F** Immunofluorescence analysis of the colocalization of CD63 with (E) TβRI or (F) TβRII in LT-HSCs freshly sorted from the BM of normal mice. Representative immunofluorescence images of three biological replicates are shown. The scale bar indicates 10 μm. Statistics of Pearson's correlation coefficient from 30 cells are (**E**) 0.839 ± 0.081 and (**F**) 0.821 ± 0.076, respectively. Data represent as the mean ± SD. **G** LT-HSCs from the BM of WT and $CD63^{-/-}$ mice were sorted in StemSpan SFEM with or without containing TGFβ1 and were incubated at 37 °C for 30 min. Then, cells were stimulated with SCF and TPO and incubated at 37 °C for another 30 min. After that, the expression of p-$Smad2^{S465/S467}$ was detected by immunofluorescence. Freshly sorted WT LT-HSCs were served as positive controls. Representative immunofluorescence images of three biological replicates are shown. The scale bar indicates 10 μm. **H**–**J** LSKs from the BM of WT and $CD63^{-/-}$ mice were transducted with lentivirus carrying control (Ctl) or CD63 gene. Then, 5×10^3 transducted LSKs (GFP^+), together with 5×10^5 CD45.1 BM helper cells, were transplanted into lethally irradiated CD45.1 recipient mice. Sixteen weeks later, (**H**) p-$Smad2^{S465/S467}$/$Smad3^{S423/S425}$ expression and (**I**) cell cycle status in donor-derived LT-HSCs, as well as (**J**) the percentage of donor-derived cells in the PB, in recipient mice were measured by flow cytometry ($n = 5$). Data are shown as the mean ± SD. $^{***}P < 0.001$, compared with WT+Ctl group; $^{\#\#\#}P < 0.001$, compared with $CD63^{-/-}$+Ctl group. **K** Schematic diagram revealing how CD63 regulates the quiescence of HSCs.

X-100. After blocking, cells were stained with anti-γ-$H2AX^{S139}$ (Biolegend), anti-p-$Smad2^{S465/S467}$ (Sigma), anti-CD63 (Abcam, Cambridge, UK), anti-TβRI (Santa Cruz, Dallas, TX, USA), or anti-TβRII (Santa Cruz) antibodies. Subsequently, some samples were stained with fluorescent dye-conjugated secondary antibodies (Invitrogen) and DAPI (Sigma) and were photographed under a Zeiss LSM800 confocal microscope (Carl Zeiss, Jena, Germany). Immunofluorescence images were analyzed using Fiji software. Pearson's correlation coefficient was used to assess the quantitation of colocalization [45, 68]. The details of the antibodies are provided in Supplementary Table S1.

Statistical analysis

All data were analyzed with GraphPad Prism 6.0 (La Jolla, CA, USA). The variance was similar within each group. Comparisons between two groups were determined by unpaired Student's *t* test (two-tailed) and differences among multiple groups were compared using one-way analysis of variance (ANOVA) followed by Tukey's test. The survival rates of mice were analyzed by log-rank test and shown as Kaplan–Meier curves. All experiments were independently performed at least three times. The numbers of biological replicates are indicated in the figure legends. The results are expressed as mean ± standard deviation (SD). $P < 0.05$ was considered statistically significant.

DATA AVAILABILITY

The datasets used and/or analyzed during the current study are available from the corresponding author on reasonable request.

REFERENCES

1. Cheng H, Zheng Z, Cheng T. New paradigms on hematopoietic stem cell differentiation. Protein Cell. 2020;11:34–44.
2. Will B, Vogler TO, Bartholdy B, Garrett-Bakelman F, Mayer J, Barreyro L, et al. Satb1 regulates the self-renewal of hematopoietic stem cells by promoting quiescence and repressing differentiation commitment. Nat Immunol. 2013;14:437–45.
3. Zhao M, Perry JM, Marshall H, Venkatraman A, Qian P, He XC, et al. Megakaryocytes maintain homeostatic quiescence and promote post-injury regeneration of hematopoietic stem cells. Nat Med. 2014;20:1321–6.
4. Boulais PE, Frenette PS. Making sense of hematopoietic stem cell niches. Blood. 2015;125:2621–9.
5. Sinha S, Dwivedi TR, Yengkhom R, Bheemsetty VA, Abe T, Kiyonari H, et al. Asrij/OCIAD1 suppresses CSN5-mediated p53 degradation and maintains mouse hematopoietic stem cell quiescence. Blood. 2019;133:2385–2400.
6. Liu L, Inoki A, Fan K, Mao F, Shi G, Jin X, et al. ER-associated degradation preserves hematopoietic stem cell quiescence and self-renewal by restricting mTOR activity. Blood. 2020;136:2975–86.
7. Venkatraman A, He XC, Thorvaldsen JL, Sugimura R, Perry JM, Tao F, et al. Maternal imprinting at the H19-Igf2 locus maintains adult haematopoietic stem cell quiescence. Nature. 2013;500:345–9.
8. Riether C, Schurch CM, Ochsenbein AF. Regulation of hematopoietic and leukemic stem cells by the immune system. Cell Death Differ. 2015;22:187–98.
9. Haas S, Trumpp A, Milsom MD. Causes and consequences of hematopoietic stem cell heterogeneity. Cell Stem Cell. 2018;22:627–38.
10. Mansell E, Sigurdsson V, Deltcheva E, Brown J, James C, Miharada K, et al. Mitochondrial potentiation ameliorates age-related heterogeneity in hematopoietic stem cell function. Cell Stem Cell. 2021;28:241–56 e246.
11. Crisan M, Dzierzak E. The many faces of hematopoietic stem cell heterogeneity. Development. 2016;143:4571–81.
12. Shin JY, Hu W, Naramura M, Park CY. High c-Kit expression identifies hematopoietic stem cells with impaired self-renewal and megakaryocytic bias. J Exp Med. 2014;211:217–31.
13. Naka K, Hirao A. Regulation of hematopoiesis and hematological disease by TGF-beta family signaling molecules. Cold Spring Harb Perspect. Biol. 2017;9:a027987.
14. Capron C, Lacout C, Lecluse Y, Jalbert V, Chagraoui H, Charrier S, et al. A major role of TGF-beta1 in the homing capacities of murine hematopoietic stem cell/progenitors. Blood. 2010;116:1244–53.
15. Blank U, Karlsson S. TGF-beta signaling in the control of hematopoietic stem cells. Blood. 2015;125:3542–50.
16. Brenet F, Kermani P, Spektor R, Rafii S, Scandura JM. TGFbeta restores hematopoietic homeostasis after myelosuppressive chemotherapy. J Exp Med. 2013;210:623–39.
17. Zhang H, Kozono DE, O'Connor KW, Vidal-Cardenas S, Rousseau A, Hamilton A, et al. TGF-beta inhibition rescues hematopoietic stem cell defects and bone marrow failure in Fanconi anemia. Cell Stem Cell 2016;18:668–81.
18. Challen GA, Boles NC, Chambers SM, Goodell MA. Distinct hematopoietic stem cell subtypes are differentially regulated by TGF-beta1. Cell Stem Cell. 2010;6:265–78.
19. Gekas C, Graf T. CD41 expression marks myeloid-biased adult hematopoietic stem cells and increases with age. Blood. 2013;121:4463–72.
20. Nakamura-Ishizu A, Matsumura T, Stumpf PS, Umemoto T, Takizawa H, Takihara Y, et al. Thrombopoietin metabolically primes hematopoietic stem cells to megakaryocyte-lineage differentiation. Cell Rep. 2018;25:1772–85 e1776.
21. Chen X, Deng H, Churchill MJ, Luchsinger LL, Du X, Chu TH, et al. Bone marrow myeloid cells regulate myeloid-biased hematopoietic stem cells via a histamine-dependent feedback loop. Cell Stem Cell. 2017;21:747–60 e747.
22. Liang R, Arif T, Kalmykova S, Kasianov A, Lin M, Menon V, et al. Restraining lysosomal activity preserves hematopoietic stem cell quiescence and potency. Cell Stem Cell. 2020;26:359–76 e357.
23. Pols MS, Klumperman J. Trafficking and function of the tetraspanin CD63. Exp Cell Res. 2009;315:1584–92.
24. Kraft S, Jouvin MH, Kulkarni N, Kissing S, Morgan ES, Dvorak AM, et al. The tetraspanin CD63 is required for efficient IgE-mediated mast cell degranulation and anaphylaxis. J Immunol. 2013;191:2871–8.
25. Israels SJ, McMillan-Ward EM. Palmitoylation supports the association of tetraspanin CD63 with CD9 and integrin alphaIIbbeta3 in activated platelets. Thromb Res. 2010;125:152–8.
26. Kobuch J, Cui H, Grunwald B, Saftig P, Knolle PA, Kruger A. TIMP-1 signaling via CD63 triggers granulopoiesis and neutrophilia in mice. Haematologica. 2015;100:1005–13.
27. Doyle EL, Ridger V, Ferraro F, Turmaine M, Saftig P, Cutler DF. CD63 is an essential cofactor to leukocyte recruitment by endothelial P-selectin. Blood. 2011;118:4265–73.
28. Beckmann J, Scheitza S, Wernet P, Fischer JC, Giebel B. Asymmetric cell division within the human hematopoietic stem and progenitor cell compartment: identification of asymmetrically segregating proteins. Blood. 2007;109:5494–501.

29. Loeffler D, Wehling A, Schneiter F, Zhang Y, Muller-Botticher N, Hoppe PS, et al. Asymmetric lysosome inheritance predicts activation of haematopoietic stem cells. Nature. 2019;573:426–9.
30. Rodriguez-Fraticelli AE, Wolock SL, Weinreb CS, Panero R, Patel SH, Jankovic M, et al. Clonal analysis of lineage fate in native haematopoiesis. Nature. 2018;553:212–6.
31. Lin KK, Rossi L, Boles NC, Hall BE, George TC, Goodell MA. CD81 is essential for the re-entry of hematopoietic stem cells to quiescence following stress-induced proliferation via deactivation of the Akt pathway. PLoS Biol. 2011;9:e1001148.
32. Wilson NK, Kent DG, Buettner F, Shehata M, Macaulay IC, Calero-Nieto FJ, et al. Combined single-cell functional and gene expression analysis resolves heterogeneity within stem cell populations. Cell Stem Cell. 2015;16:712–24.
33. Mohrin M, Shin J, Liu Y, Brown K, Luo H, Xi Y, et al. Stem cell aging. A mitochondrial UPR-mediated metabolic checkpoint regulates hematopoietic stem cell aging. Science. 2015;347:1374–7.
34. Ho TT, Warr MR, Adelman ER, Lansinger OM, Flach J, Verovskaya EV, et al. Autophagy maintains the metabolism and function of young and old stem cells. Nature. 2017;543:205–10.
35. Sanjuan-Pla A, Macaulay IC, Jensen CT, Woll PS, Luis TC, Mead A, et al. Platelet-biased stem cells reside at the apex of the haematopoietic stem-cell hierarchy. Nature. 2013;502:232–6.
36. Theilgaard-Monch K, Jacobsen LC, Nielsen MJ, Rasmussen T, Udby L, Gharib M, et al. Haptoglobin is synthesized during granulocyte differentiation, stored in specific granules, and released by neutrophils in response to activation. Blood. 2006;108:353–61.
37. Tidwell T, Wechsler J, Nayak RC, Trump L, Salipante SJ, Cheng JC, et al. Neutropenia-associated ELANE mutations disrupting translation initiation produce novel neutrophil elastase isoforms. Blood. 2014;123:562–9.
38. Schroder J, Lullmann-Rauch R, Himmerkus N, Pleines I, Nieswandt B, Orinska Z, et al. Deficiency of the tetraspanin CD63 associated with kidney pathology but normal lysosomal function. Mol Cell Biol. 2009;29:1083–94.
39. Komorowska K, Doyle A, Wahlestedt M, Subramaniam A, Debnath S, Chen J, et al. Hepatic leukemia factor maintains quiescence of hematopoietic stem cells and protects the stem cell pool during regeneration. Cell Rep. 2017;21:3514–23.
40. Velardi E, Tsai JJ, Radtke S, Cooper K, Argyropoulos KV, Jae-Hung S, et al. Suppression of luteinizing hormone enhances HSC recovery after hematopoietic injury. Nat Med. 2018;24:239–46.
41. Baumgartner C, Toifl S, Farlik M, Halbritter F, Scheicher R, Fischer I, et al. An ERK-dependent feedback mechanism prevents hematopoietic stem cell exhaustion. Cell Stem Cell. 2018;22:879–92 e876.
42. Borges L, Oliveira VKP, Baik J, Bendall SC, Perlingeiro RCR. Serial transplantation reveals a critical role for endoglin in hematopoietic stem cell quiescence. Blood. 2019;133:688–96.
43. Miyagi S, Sroczynska P, Kato Y, Nakajima-Takagi Y, Oshima M, Rizq O, et al. The chromatin-binding protein Phf6 restricts the self-renewal of hematopoietic stem cells. Blood. 2019;133:2495–506.
44. Yamazaki S, Iwama A, Takayanagi S, Eto K, Ema H, Nakauchi H. TGF-beta as a candidate bone marrow niche signal to induce hematopoietic stem cell hibernation. Blood. 2009;113:1250–6.
45. Hermetet F, Buffiere A, Aznague A, Pais de Barros JP, Bastie JN, Delva L, et al. High-fat diet disturbs lipid raft/TGF-beta signaling-mediated maintenance of hematopoietic stem cells in mouse bone marrow. Nat Commun. 2019;10:523.
46. Leiva M, Quintana JA, Ligos JM, Hidalgo A. Haematopoietic ESL-1 enables stem cell proliferation in the bone marrow by limiting TGFbeta availability. Nat Commun. 2016;7:10222.
47. Balise VD, Saito-Reis CA, Gillette JM. Tetraspanin scaffold proteins function as key regulators of hematopoietic stem cells. Front Cell Dev Biol. 2020;8:598.
48. Lam J, van den Bosch M, Wegrzyn J, Parker J, Ibrahim R, Slowski K, et al. miR-143/145 differentially regulate hematopoietic stem and progenitor activity through suppression of canonical TGFbeta signaling. Nat Commun. 2018;9:2418.
49. Jiang L, Han X, Wang J, Wang C, Sun X, Xie J, et al. SHP-1 regulates hematopoietic stem cell quiescence by coordinating TGF-beta signaling. J Exp Med. 2018;215:1337–47.
50. Shao L, Elujoba-Bridenstine A, Zink KE, Sanchez LM, Cox BJ, Pollok KE, et al. The neurotransmitter receptor Gabbr1 regulates proliferation and function of hematopoietic stem and progenitor cells. Blood. 2021;137:775–87.
51. Xiong Z, Xia P, Zhu X, Geng J, Wang S, Ye B, et al. Glutamylation of deubiquitinase BAP1 controls self-renewal of hematopoietic stem cells and hematopoiesis. J Exp Med. 2020;217:e20190974.
52. Land RH, Rayne AK, Vanderbeck AN, Barlowe TS, Manjunath S, Gross M, et al. The orphan nuclear receptor NR4A1 specifies a distinct subpopulation of quiescent myeloid-biased long-term HSCs. Stem Cells. 2015;33:278–88.
53. Cabezas-Wallscheid N, Buettner F, Sommerkamp P, Klimmeck D, Ladel L, Thalheimer FB, et al. Vitamin A-retinoic acid signaling regulates hematopoietic stem cell dormancy. Cell. 2017;169:807–23 e819.
54. Larochelle A, Savona M, Wiggins M, Anderson S, Ichwan B, Keyvanfar K, et al. Human and rhesus macaque hematopoietic stem cells cannot be purified based only on SLAM family markers. Blood. 2011;117:1550–4.
55. Sadej R, Romanska H, Kavanagh D, Baldwin G, Takahashi T, Kalia N, et al. Tetraspanin CD151 regulates transforming growth factor beta signaling: implication in tumor metastasis. Cancer Res. 2010;70:6059–70.
56. Seubert B, Cui H, Simonavicius N, Honert K, Schafer S, Reuning U, et al. Tetraspanin CD63 acts as a pro-metastatic factor via beta-catenin stabilization. Int J Cancer. 2015;136:2304–15.
57. Toricelli M, Melo FH, Peres GB, Silva DC, Jasiulionis MG. Timp1 interacts with beta-1 integrin and CD63 along melanoma genesis and confers anoikis resistance by activating PI3-K signaling pathway independently of Akt phosphorylation. Mol Cancer. 2013;12:22.
58. Ni F, Yu WM, Wang X, Fay ME, Young KM, Qiu Y, et al. Ptpn21 controls hematopoietic stem cell homeostasis and biomechanics. Cell Stem Cell. 2019;24:608–20 e606.
59. Quere R, Saint-Paul L, Carmignac V, Martin RZ, Chretien ML, Largeot A, et al. Tif1gamma regulates the TGF-beta1 receptor and promotes physiological aging of hematopoietic stem cells. Proc Natl Acad Sci USA. 2014;111:10592–7.
60. Park SM, Deering RP, Lu Y, Tivnan P, Lianoglou S, Al-Shahrour F, et al. Musashi-2 controls cell fate, lineage bias, and TGF-beta signaling in HSCs. J Exp Med. 2014;211:71–87.
61. Rossi L, Ergen AV, Goodell MA. TIMP-1 deficiency subverts cell-cycle dynamics in murine long-term HSCs. Blood. 2011;117:6479–88.
62. Hu M, Zeng H, Chen S, Xu Y, Wang S, Tang Y, et al. SRC-3 is involved in maintaining hematopoietic stem cell quiescence by regulation of mitochondrial metabolism in mice. Blood. 2018;132:911–23.
63. Hu M, Lu Y, Zeng H, Zhang Z, Chen S, Qi Y, et al. MicroRNA-21 maintains hematopoietic stem cell homeostasis through sustaining the NF-kappaB signaling pathway in mice. Haematologica. 2021;106:412–23.
64. Chen Z, Huo D, Li L, Liu Z, Li Z, Xu S, et al. Nuclear DEK preserves hematopoietic stem cells potential via NCoR1/HDAC3-Akt1/2-mTOR axis. J Exp Med. 2021;218:e20201974.
65. Zeng H, Hu M, Lu Y, Zhang Z, Xu Y, Wang S, et al. MicroRNA 34a promotes ionizing radiation-induced DNA damage repair in murine hematopoietic stem cells. FASEB J. 2019;33:8138–47.
66. Nakagawa MM, Rathinam CV. Constitutive activation of the canonical NF-kappaB pathway leads to bone marrow failure and induction of erythroid signature in hematopoietic stem cells. Cell Rep. 2018;25:2094–109 e2094.
67. Hu M, Lu Y, Qi Y, Zhang Z, Wang S, Xu Y, et al. SRC-3 functions as a coactivator of T-bet by regulating the maturation and antitumor activity of natural killer cells. Cancer Immunol Res. 2020;8:1150–62.
68. Adler J, Parmryd I. Quantifying colocalization by correlation: the Pearson correlation coefficient is superior to the Mander's overlap coefficient. Cytometry A 2010;77:733–42.

ACKNOWLEDGEMENTS

The authors thank Prof. Jinyong Wang (Guangzhou Institutes of Biomedicine and Health, Chinese Academy of Science) for gifting CD45.1 mice, Yang Liu (The Third Military Medical University) for technical support in flow cytometry and Liting Wang (The Third Military Medical University) for technical support in immunofluorescence microscopy.

AUTHOR CONTRIBUTIONS

M.H. designed the study, performed experiments, analyzed data, and wrote the paper. Y.L., S.W., Z.Z., and Y.Q. performed some experiments and analyzed data. N.C., M.S., and F.C. participated in some in vitro experiments. M.C., L.Y., and S.C. participated data analysis. D.Z., F.W., and Y.S. participated in the initial experimental design and discussed the manuscript. Y.X. and J.W. jointly conceived and supervised the study, and revised the manuscript. All authors read and approved the final paper.

FUNDING

This work was supported by grants from the National Natural Science Fund of China (No. 81725019, 81930090, and 81573084) and the Scientific Research Project of PLA (No. ALJ19J002 and AWS16J014).

ETHICS STATEMENT

This study was approved by the Animal Care Committee of The Third Military Medical University (no. AMUWEC20191824).

COMPETING INTERESTS

The authors declare no competing interests.

ADDITIONAL INFORMATION

Supplementary information The online version contains supplementary material available at https://doi.org/10.1038/s41418-021-00848-2.

Correspondence and requests for materials should be addressed to Y.X. or J.W.